

# Counterpropagating continuous-variable entangled states in lossy coupled-cavity optical waveguides

Hossein Seifoory,<sup>1,\*</sup> L. G. Helt,<sup>1</sup> J. E. Sipe,<sup>2</sup> and Marc M. Dignam<sup>1</sup>

<sup>1</sup>*Department of Physics, Engineering Physics and Astronomy, Queen's University, Kingston, Ontario, Canada K7L 3N6*

<sup>2</sup>*Department of Physics and Institute for Optical Sciences, University of Toronto, 60 St. George Street, Toronto, Ontario, Canada M5S 1A7*



(Received 28 June 2019; published 30 September 2019)

We present an integrated source of counterpropagating entangled states based on a coupled resonator optical waveguide that is pumped by a classical pulsed source incident from above the waveguide. We investigate theoretically the generation and propagation of continuous-variable entangled states in this coupled-cavity system in the presence of intrinsic loss. Using a tight-binding approximation, we derive analytic time-dependent expressions for the number of photons in each cavity, as well as for the correlation variance between the photons in different pairs of cavities, to evaluate the degree of quantum entanglement. We also derive simple approximate expressions for these quantities that can be used to guide the design of such systems, and discuss how pumping configurations and physical properties of the system affect the photon statistics and the degree of quantum correlation.

DOI: [10.1103/PhysRevA.100.033839](https://doi.org/10.1103/PhysRevA.100.033839)

## I. INTRODUCTION

Entangled quantum states have potential applications in quantum teleportation [1,2], quantum computation, and quantum information [3,4]. They can either involve discrete variables (DVs), such as the polarization of a photon, or continuous variables (CVs), such as the quadratures of a beam of light. Although DV systems provide high-fidelity operations, photonic-based DV entanglement is currently limited by the difficulties of single-photon generation and detection, and by high sensitivity to optical losses. In contrast, CV entanglement is more robust to loss, and can be more efficiently created and used for the implementation of quantum protocols [5–9]. Spontaneous parametric down conversion (SPDC), a second-order nonlinear process in which a pump photon is converted into a signal and an idler photon, is one of the processes that can be used to generate quantum correlated states [10–12]. It has been implemented in both bulk media and integrated photonic structures. However, as the size and complexity of quantum information processing systems increase, the limitations in achieving stability, precision, and small physical size with bulk optical systems become significant. Systems for on-chip SPDC, which are integrable with other photonic elements and could be used to generate CV entangled states involving two spatially separated sites, are therefore very promising [13–15].

One such platform involves the use of waveguides made of materials with a large second-order nonlinear optical response, such as AlGaAs, to generate counterpropagating, quantum correlated photons [16,17]. The particular system we consider here is the coupled-resonator optical waveguide (CROW), in which the waveguide consists of optical cavities weakly coupled in one dimension. By adjusting the nature of the cavities and the coupling between them, the dispersive

properties of the propagating modes can be controlled [18]. Loss, which can destroy the nonclassical properties of light [19–23], can also be controlled to some extent, allowing at least a partial optimization for particular applications. CROW structures have been shown to have potential in generating CV entangled states between two side cavities coupled to the CROW, and as well between spatially separated sites [13]. It is the latter application we study here.

Our integrated source of entangled states is schematically shown in Fig. 1. A pump pulse is incident on a set of central cavities from above. Consequently, in order for the phase matching condition to be fulfilled, the generated signal and idler modes propagate in opposite directions in the CROW structure. An important advantage of such a configuration is the absence of the pump mode in the guided direction. Moreover, it has also been shown that the properties of the counterpropagating guided signal and idler modes can be tuned using the spectral and spatial properties of the pump [17,24,25].

The tight-binding (TB) method [26,27], which uses localized single-cavity modes as a basis, can be applied to model the evolution of light in such a coupled structure. Assuming that all the cavities are identical and support the same mode with complex frequency  $\tilde{\omega}_F$ , it has been shown [28] that in the nearest-neighbor tight-binding (NNTB) approximation the dispersion relation can be written as

$$\begin{aligned}\tilde{\omega}_{Fk} &\approx \tilde{\omega}_F [1 - \tilde{\beta}_1 \cos(kD)] \\ &\equiv \omega_{Fk} - i\gamma_{Fk},\end{aligned}\quad (1)$$

where  $\tilde{\beta}_1$ ,  $D$ , and  $k$  are, respectively, the complex coupling parameter, the periodicity of the CROW, and the Bloch vector component. The imaginary part of the complex frequency is associated with the loss of the Bloch modes in the CROW. It is clear from Eq. (1) that these modes experience different loss rates; it has been shown that the rates can differ by an order of magnitude or more [22,29,30].

\*hossein.seifoory@queensu.ca

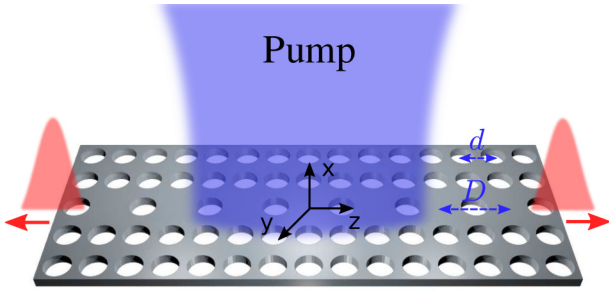


FIG. 1. Schematic picture of the particular CROW structure with period  $D$  formed from defects in a slab photonic crystal with a square lattice of period  $d$  and height  $h$ . The blue region shows the region covered by the pump. The origin of the coordinate system is at the center of the slab, i.e., the center of the central cavity.

In our previous work we focused on the time evolution of a state generated in a coupled-cavity system, and studied the evolution and propagation of squeezing and entanglement [22]. We presented analytic expressions for a general initial state, but only presented detailed results for an initial state that was a squeezed vacuum state in one of the cavities. In this work we investigate both the generation and propagation of entangled states in coupled-cavity systems. In addition, we engineer the pump parameters to produce counterpropagating pulses of the generated signal and idler modes, which are entangled but are not individually squeezed. Including the effects of intrinsic propagation loss, we calculate the number of photons in each cavity and the CV correlation variance of photons in different cavities.

Previous approaches for generating counterpropagating entangled states have focused on photon pairs and been based either on ridge waveguides with vertical pumping [16,17], or on periodic waveguides with horizontal pumping [31]. The new approach of using a CROW has a number of advantages. First, the CROW allows us to control the group velocity and the frequency at which there is zero group velocity dispersion. Second, because a CROW can be modeled using a TB method, we are able to specify and model the effects of intrinsic scattering loss on the generated CV entanglement as a function of propagation distance, which is important for any application. Finally, using vertical pumping leads to counterpropagating entangled states, with no copropagating pump at the outputs.

This paper is organized as follows. In Sec. II we present the general theory of the generation and the evolution of the generalized two mode squeezed state in lossy CROWs via SPDC. In Sec. III we consider the special case of a pump that is Gaussian in time and space, and derive analytic expressions for the time dependence of the number of photons and the CV correlations. In Sec. IV we present our results for a particular CROW in a slab photonic crystal, and discuss how they might be affected by the pumping configuration and the physical properties of the structure. Finally, in Sec. V we present our conclusions.

## II. GENERAL THEORY

In order to determine both the generation and evolution of the entangled squeezed states in the system, we divide the

analysis into two separate tasks. First, we study the creation of the entangled photons via SPDC using the backward Heisenberg method [32], which is intrinsically a lossless approach. Having determined the initial entangled states created by the pump, we then include the loss to see how the generated state evolves in time and how loss affects it. Note that this two-step approach is valid because, for the parameters considered in this paper, the pump pulse is short enough that the signal loss is negligible over its duration.

### A. Generation

There are two mode types that are relevant here, the fundamental modes and the pump modes; we indicate them by  $F$  and  $S$ , respectively. In the SPDC process, two photons are generated in  $F$  modes from one pump photon in mode  $S$ . Expanding the full displacement field  $\mathbf{D}(\mathbf{r})$  in terms of the modes of interest, we have

$$\mathbf{D}(\mathbf{r}) = \left( \int dk \sqrt{\frac{\hbar\omega_{Fk}}{2}} \mathbf{D}_{Fk}(\mathbf{r}) \hat{a}_{Fk} + \sum_m \int d\mathbf{q} \sqrt{\frac{\hbar\omega_{Smq}}{2}} \mathbf{M}_{Smq}(\mathbf{r}) \hat{a}_{Smq} \right) + \text{H.c.}, \quad (2)$$

where  $\mathbf{M}_{Smq}$ ,  $\omega_{Smq}$ , and  $\hat{a}_{Smq}$  are the modes, eigenfrequencies, and annihilation operators of the pump field, respectively, and  $\mathbf{D}_{Fk}$ ,  $\omega_{Fk}$ , and  $\hat{a}_{Fk}$  are the corresponding quantities for the generated signal and idler fields. Note that the integral over  $k$  in Eq. (2) and in the rest of the paper (except where explicitly noted) only ranges from  $-\pi/D$  to  $\pi/D$ . The continuous index  $\mathbf{q}$  is to identify the different pump modes in three dimensions (3D) while  $m$  identifies the polarization state. The normalization conditions for the modes are presented in Appendix A. Here

$$\begin{aligned} [\hat{a}_{Fk}, \hat{a}_{Smq}^\dagger] &= [\hat{a}_{Fk}, \hat{a}_{Smq}] = 0, \\ [\hat{a}_{Smq}, \hat{a}_{Smq'}^\dagger] &= \delta_{mm'} \delta(\mathbf{q} - \mathbf{q}'), \\ [\hat{a}_{Fk}, \hat{a}_{Fk'}^\dagger] &= \delta(k - k'). \end{aligned} \quad (3)$$

For convenience we put

$$\hat{a}_{Fk} \rightarrow \hat{b}_k, \quad \hat{a}_{Smq} \rightarrow \hat{c}_{mq}, \quad (4)$$

and the linear Hamiltonian is then given by

$$H_L = \int dk \hbar\omega_{Fk} \hat{b}_k^\dagger \hat{b}_k + \sum_m \int d\mathbf{q} \hbar\omega_{Smq} \hat{c}_{mq}^\dagger \hat{c}_{mq}, \quad (5)$$

where we neglect the zero point energy and use only the real part of  $\omega_{Fk}$  for the mode frequency. The nonlinear Hamiltonian that should be added to  $H_L$  to construct the full Hamiltonian is [32]

$$H_{NL} = - \sum_m \int dk_1 dk_2 d\mathbf{q} S(k_1, k_2, m, \mathbf{q}) \hat{b}_{k_1}^\dagger \hat{b}_{k_2}^\dagger \hat{c}_{mq} + \text{H.c.}, \quad (6)$$

where  $S(k_1, k_2, m, \mathbf{q})$  is the coupling coefficient, which is given by

$$S(k_1, k_2, m, \mathbf{q}) = \frac{1}{\varepsilon_0} \sqrt{\frac{\hbar \omega_{Fk_1} \hbar \omega_{Fk_2} \hbar \omega_{Sm\mathbf{q}}}{8}} \int d\mathbf{r} \chi_2^{ijk}(\mathbf{r}) \times \frac{[D_{Fk_1}^i(\mathbf{r}) D_{Fk_2}^j(\mathbf{r})]^* M_{Sm\mathbf{q}}^k(\mathbf{r})}{\varepsilon_0 n^2(\mathbf{r}; \omega_{Fk_1}) n^2(\mathbf{r}; \omega_{Fk_2}) n^2(\mathbf{r}; \omega_{Sm\mathbf{q}})}, \quad (7)$$

where  $n(\mathbf{r}; \omega)$  is a real, position and frequency-dependent refractive index and  $\chi_2^{ijk}(\mathbf{r})$  is the position-dependent second-order nonlinear susceptibility.

We take the pump to be a classical pulse incident on the slab, which we can expand as a superposition of the pump modes  $M_{Sm\mathbf{q}}(\mathbf{r})$ . We borrow a strategy from Yang *et al.* [32] and define asymptotic-in and asymptotic-out states to be, respectively, the input and output states of the nonlinear region at  $t = 0$ , taking  $t = 0$  to be the time when the pump is centered on the slab. For the asymptotic-in state  $|\psi_{\text{in}}\rangle$  that describes the classical pump pulse as a coherent state, we have

$$|\psi_{\text{in}}\rangle = e^{\alpha \sum_m \int d\mathbf{q} \phi_P(m, \mathbf{q}) \hat{c}_{m\mathbf{q}}^\dagger - \text{H.c.}} |\text{vac}\rangle, \quad (8)$$

where  $\alpha$  is a complex number, and we normalize the complex function  $\phi_P(m, \mathbf{q})$  according to

$$\sum_m \int d\mathbf{q} |\phi_P(m, \mathbf{q})|^2 = 1. \quad (9)$$

The expectation value of the displacement field of the pump pulse is then

$$\langle \psi_{\text{in}} | \mathbf{D}(\mathbf{r}) | \psi_{\text{in}} \rangle = \alpha \sum_m \int d\mathbf{q} \sqrt{\frac{\hbar \omega_{Sm\mathbf{q}}}{2}} \phi_P(m, \mathbf{q}) \mathbf{M}_{Sm\mathbf{q}}(\mathbf{r}) + \text{c.c.} \quad (10)$$

and since

$$\langle \psi_{\text{in}} | \hat{c}_{m\mathbf{q}}^\dagger \hat{c}_{m\mathbf{q}} | \psi_{\text{in}} \rangle = |\alpha|^2 |\phi_P(m, \mathbf{q})|^2 \quad (11)$$

we can identify  $|\alpha|^2$  as the expectation value of the number of photons in the pump pulse. Following the backward Heisenberg picture approach [32], the asymptotic-out state for the generated photons in the first approximation is then

$$|\psi_{\text{out}}^F\rangle = e^{\frac{\beta}{\sqrt{2}} \int dk_1 dk_2 \phi(k_1, k_2) \hat{b}_{k_1}^\dagger \hat{b}_{k_2}^\dagger - \text{H.c.}} |\text{vac}\rangle, \quad (12)$$

where  $\phi(k_1, k_2)$  is the biphoton wave function, which from Yang *et al.* [32] is given by

$$\phi(k_1, k_2) = \frac{2i\sqrt{2}\pi\alpha}{\beta\hbar} \sum_m \int d\mathbf{q} \phi_P(m, \mathbf{q}) \times S(k_1, k_2, m, \mathbf{q}) \delta(\omega_{Sm\mathbf{q}} - \omega_{Fk_1} - \omega_{Fk_2}), \quad (13)$$

where  $\beta$  is a real and positive normalization constant chosen to ensure that  $\int dk_1 dk_2 |\phi(k_1, k_2)|^2 = 1$ .

While the biphoton wave function in general obeys the symmetry  $\phi(k_1, k_2) = \phi(k_2, k_1)$ , it can sometimes be useful to work with a function that breaks this symmetry to focus attention on a particular quadrant of  $(k_1, k_2)$  space. In this work we will always choose the pump parameters such that to a very good approximation,  $\phi(k_1, k_2)$  is nonzero only when

$k_1$  and  $k_2$  have opposite signs, as we detail in Sec. III below. Then we can write

$$\begin{aligned} & \int_{-\pi/D}^{\pi/D} dk_1 \int_{-\pi/D}^{\pi/D} dk_2 \phi(k_1, k_2) \hat{b}_{k_1}^\dagger \hat{b}_{k_2}^\dagger \\ & \approx \int_0^{\pi/D} dk_1 \int_{-\pi/D}^0 dk_2 \phi(k_1, k_2) \hat{b}_{k_1}^\dagger \hat{b}_{k_2}^\dagger \\ & + \int_{-\pi/D}^0 dk_1 \int_0^{\pi/D} dk_2 \phi(k_1, k_2) \hat{b}_{k_1}^\dagger \hat{b}_{k_2}^\dagger \\ & = 2 \int_0^{\pi/D} dk_1 \int_{-\pi/D}^0 dk_2 \phi(k_1, k_2) \hat{b}_{k_1}^\dagger \hat{b}_{k_2}^\dagger. \end{aligned} \quad (14)$$

We then define

$$\Phi(k_1, k_2) \equiv \sqrt{2} \phi(k_1, k_2) \Theta(k_1) \Theta(-k_2), \quad (15)$$

where  $\Theta(k)$  is the Heaviside function, such that we may rewrite Eq. (12) as

$$|\psi_{\text{out}}^F\rangle = e^{\beta \int dk_1 dk_2 \Phi(k_1, k_2) \hat{b}_{k_1}^\dagger \hat{b}_{k_2}^\dagger - \text{H.c.}} |\text{vac}\rangle. \quad (16)$$

Employing a Schmidt decomposition [33,34], we have

$$\Phi(k_1, k_2) = \sum_\lambda \sqrt{p_\lambda} \mu_\lambda(k_1) \nu_\lambda(k_2), \quad (17)$$

for  $p_\lambda > 0$  with  $\sum_\lambda p_\lambda = 1$ , where the Schmidt functions are orthonormal,

$$\int dk \mu_\lambda(k) \mu_{\lambda'}^*(k) = \int dk \nu_\lambda(k) \nu_{\lambda'}^*(k) = \delta_{\lambda, \lambda'}. \quad (18)$$

We extend the sets of  $\mu_\lambda(k)$  and  $\nu_\lambda(k)$  associated with  $p_\lambda > 0$  to form complete sets with

$$\sum_\lambda \mu_\lambda(k) \mu_\lambda^*(k') = \sum_\lambda \nu_\lambda(k) \nu_\lambda^*(k') = \delta(k - k'), \quad (19)$$

and with some of the  $p_\lambda$  appearing in Eq. (17) then equal to zero. Using Eqs. (16) and (17), the generated squeezed state can be written as

$$|\psi_{\text{out}}^F\rangle = \hat{S} |\text{vac}\rangle, \quad (20)$$

where the squeezing operator  $\hat{S}$  can be written as

$$\begin{aligned} \hat{S} &= \exp \left( \beta \int dk_1 dk_2 \sum_\lambda \sqrt{p_\lambda} \mu_\lambda(k_1) \nu_\lambda(k_2) \hat{b}_{k_1}^\dagger \hat{b}_{k_2}^\dagger - \text{H.c.} \right) \\ &= \exp \left( \sum_\lambda r_\lambda \hat{B}_\lambda^\dagger \hat{C}_\lambda^\dagger - \sum_\lambda r_\lambda^* \hat{B}_\lambda \hat{C}_\lambda \right), \end{aligned} \quad (21)$$

where  $r_\lambda = \beta \sqrt{p_\lambda}$  is the squeezing parameter,

$$\hat{B}_\lambda \equiv \int \mu_\lambda^*(k) \hat{b}_k dk, \quad (22)$$

and

$$\hat{C}_\lambda \equiv \int \nu_\lambda^*(k) \hat{b}_k dk. \quad (23)$$

Using Eq. (19), it can be shown that  $[\hat{B}_\lambda, \hat{B}_{\lambda'}^\dagger] = [\hat{C}_\lambda, \hat{C}_{\lambda'}^\dagger] = \delta_{\lambda, \lambda'}$  and  $[\hat{B}_\lambda, \hat{C}_{\lambda'}^\dagger] = [\hat{B}_{\lambda'}^\dagger, \hat{C}_\lambda] = [\hat{C}_\lambda, \hat{C}_{\lambda'}] = [\hat{B}_\lambda, \hat{C}_{\lambda'}] = 0$ .

The importance of the Schmidt decomposition and the operator transformation is that it enables us to express the generated state as a generalized two-mode squeezed state, where the modes are no longer the Bloch modes. As we shall see in the next section, this will enable us to easily determine the evolution of the state in the presence of loss.

### B. Evolution

As mentioned earlier, we have assumed that the loss during the generation process is negligible. However, the effect of loss cannot be ignored when calculating the evolution of the generated pulses down the CROW.

Following the formalism presented in our previous work [22] on lossy coupled-cavity systems, the individual single-mode cavity annihilation operator for the  $p$ th cavity,  $\hat{a}_p$ , can be written in terms of the  $k$ th mode annihilation operator of the coupled-cavity system  $\hat{b}_k$  as

$$\hat{a}_p(t) = \sqrt{\frac{D}{2\pi}} \int \hat{b}_k(t) e^{ikpD} dk. \quad (24)$$

The time evolution of the full coupled-cavity annihilation operator can also be found by solving the adjoint master equation for this open, lossy system [35]. We have previously shown that the time dependence of the individual annihilation operators is given by

$$\hat{b}_k(t) = \hat{b}_k e^{-i\tilde{\omega}_F t}, \quad (25)$$

where  $\hat{b}_k = \hat{b}_k(0)$  is the corresponding operator in the Schrödinger representation [36]. Using Eqs. (24), (25), and their complex conjugates, the time-dependent average photon number in the  $p$ th cavity can be written as

$$\begin{aligned} \langle \hat{a}_p^\dagger(t) \hat{a}_p(t) \rangle &= \frac{D}{2\pi} \iint dk dk' \langle \hat{b}_k^\dagger \hat{b}_{k'} \rangle e^{-i(k-k')pD} \\ &\times (e^{i\tilde{\omega}_F^* [1-\tilde{\beta}_1^* \cos(kD)]t} e^{-i\tilde{\omega}_F [1-\tilde{\beta}_1 \cos(k'D)]t}), \end{aligned} \quad (26)$$

where we have used the lossy dispersion relation of the CROW structure [Eq. (1)]. To facilitate the evaluation of  $\langle \hat{b}_k^\dagger \hat{b}_{k'} \rangle$ , we introduce the restricted operators,

$$\begin{aligned} \hat{b}_{k,+} &\equiv \Theta(k) \hat{b}_k, \\ \hat{b}_{k,-} &\equiv \Theta(-k) \hat{b}_k. \end{aligned} \quad (27)$$

Using these operators, we can write

$$\langle \hat{b}_k^\dagger \hat{b}_{k'} \rangle = \langle \hat{b}_{k,+}^\dagger \hat{b}_{k',-} + \hat{b}_{k,-}^\dagger \hat{b}_{k',-} + \hat{b}_{k,+}^\dagger \hat{b}_{k',+} + \hat{b}_{k,-}^\dagger \hat{b}_{k',+} \rangle. \quad (28)$$

To evaluate each of these terms, we use the following Bogoliubov transformations:

$$\begin{aligned} \hat{S}^\dagger \hat{b}_{k,+} \hat{S} &= \hat{S}^\dagger \sum_{\lambda} \mu_{\lambda}(k) \hat{B}_{\lambda} \hat{S} \\ &= \sum_{\lambda} \mu_{\lambda}(k) [\hat{B}_{\lambda} \cosh(r_{\lambda}) - \hat{C}_{\lambda}^\dagger \sinh(r_{\lambda})], \end{aligned} \quad (29)$$

$$\begin{aligned} \hat{S}^\dagger \hat{b}_{k,-} \hat{S} &= \hat{S}^\dagger \sum_{\lambda} \nu_{\lambda}(k) \hat{C}_{\lambda} \hat{S} \\ &= \sum_{\lambda} \nu_{\lambda}(k) [\hat{C}_{\lambda} \cosh(r_{\lambda}) - \hat{B}_{\lambda}^\dagger \sinh(r_{\lambda})]. \end{aligned} \quad (30)$$

Using these in Eq. (28), we obtain

$$\langle \hat{b}_k^\dagger \hat{b}_{k'} \rangle = \sum_{\lambda} [\mu_{\lambda}^*(k) \mu_{\lambda}(k') + \nu_{\lambda}^*(k) \nu_{\lambda}(k')] \sinh^2(r_{\lambda}). \quad (31)$$

To study the degree of entanglement between the photons in cavities  $p$  and  $p'$  in a CROW, we use the correlation variance, which is defined as

$$\Delta_{p,p'}^2 = \langle [\Delta(\hat{X}_p - \hat{X}_{p'})]^2 \rangle + \langle [\Delta(\hat{Y}_p + \hat{Y}_{p'})]^2 \rangle, \quad (32)$$

where

$$\begin{aligned} \hat{X}_p &\equiv \hat{a}_p + \hat{a}_p^\dagger, \\ \hat{Y}_p &\equiv -i(\hat{a}_p - \hat{a}_p^\dagger). \end{aligned} \quad (33)$$

It has been shown that  $\Delta_{p,p'}^2 < 4$  can be considered as the inseparability criterion for entanglement [37–40]. Using Eq. (33) in Eq. (32), the time-dependent correlation variance can be written as

$$\Delta_{p,p'}^2 = 4 + 4(\langle \hat{a}_p^\dagger \hat{a}_p \rangle + \langle \hat{a}_{p'}^\dagger \hat{a}_{p'} \rangle - \langle \hat{a}_p \hat{a}_{p'} \rangle - \langle \hat{a}_p^\dagger \hat{a}_{p'}^\dagger \rangle). \quad (34)$$

Following a procedure similar to that used to arrive at Eqs. (26) and (31), one can derive the other expectation values that are needed to evaluate the variances of the quadrature operators and the correlation variance in the CROW structure. Note that the inseparability criterion considered here, which is based on the sum of the variances, is one of several different sufficient criteria that have been employed to investigate CV entanglement [41–43]. For instance, one can use the CV inseparability criterion of Mancini *et al.* [41], which is given in terms of the product of the same variances:

$$\bar{\Delta}_{p,p'}^2 = \langle [\Delta(\hat{X}_p - \hat{X}_{p'})]^2 \rangle \langle [\Delta(\hat{Y}_p + \hat{Y}_{p'})]^2 \rangle < 4. \quad (35)$$

As we discuss in Appendix B, these two criteria give qualitatively similar results for the times over which entanglement is observed in our system. Since the criterion of Duan *et al.* gives a simpler final expression, we employ it throughout this work.

### III. RESULTS FOR A GAUSSIAN PUMP PULSE

The results of the previous sections are general and independent of the temporal and spatial form of the pump pulse, as long as  $\phi(k_1, k_2)$  is nonzero only when  $k_1$  and  $k_2$  have opposite signs. However, in this section we consider the special case of a Gaussian pump pulse incident on the slab, and brought to a Gaussian focus there.

We assume that the slab does not have a significant effect on the pump pulse, and so take the pump modes to be plane waves in free space and set  $n(\mathbf{r}, \omega_{Sm\mathbf{q}}) = 1$  in Eq. (7). Thus we have

$$\mathbf{M}_{Sm\mathbf{q}}(\mathbf{r}) = \frac{\sqrt{\epsilon_0} \mathbf{e}_{m,\mathbf{q}}}{(2\pi)^{3/2}} e^{i\mathbf{q}\cdot\mathbf{r}}, \quad (36)$$

where  $\mathbf{e}_{m,\mathbf{q}}$  is the polarization unit vector. In what follows, we assume that in the vicinity of the CROW, the pump is

polarized in the  $y$  direction. Thus we obtain

$$\phi_P(m, \mathbf{q}) = \delta_{my} \varphi(q_x) F(q_y, q_z), \quad (37)$$

where

$$F(q_y, q_z) = \frac{1}{2\pi} \int dy dz f(y, z) e^{-i(q_y y + q_z z)} \quad (38)$$

is the Fourier transform of the transverse profile

$$f(y, z) = \frac{\sqrt{2}}{\sqrt{\pi} W_S} e^{-\frac{y^2+z^2}{W_S^2}} e^{iq_P \frac{y^2+z^2}{2R_P}}, \quad (39)$$

and  $q_P$  is the value of  $q_x$  at which  $\phi(q_x)$  peaks. Here  $R_P$  and  $W_S$  are the radius of curvature and spot size, respectively, evaluated at  $x = 0$  and  $q_x = q_P$ . We have assumed the Rayleigh range to be much larger than the slab thickness, which justifies the neglect of the Gouy phase. The prefactors have been chosen so that the normalization condition Eq. (9) becomes

$$\int dq_x |\varphi(q_x)|^2 = 1. \quad (40)$$

Neglecting the dependence of the indices of refraction and the frequencies under the square root on  $k_1$ ,  $k_2$ , and  $\mathbf{q}$ , based on the small frequency range of the input pump pulse and the limited range of the signal and idler photons in the CROW, we can rewrite the biphoton wave function of Eq. (15) as

$$\begin{aligned} \Phi(k_1, k_2) &= \frac{i\alpha\sqrt{\pi}}{\beta\hbar\sqrt{\epsilon_0}} \sqrt{(\hbar\omega_F)^2 \hbar\omega_{Sy}} \int dq_x \varphi(q_x) \\ &\times \int d\mathbf{r} \chi_2^{ijy}(\mathbf{r}) \frac{[D_{Fk_1}^i(\mathbf{r}) D_{Fk_2}^j(\mathbf{r})]^* f(y, z) e^{iq_P x}}{\epsilon_0 n^4(\mathbf{r}; \omega_F)} \\ &\times \delta(cq_x - \omega_{Fk_1} - \omega_{Fk_2}) \Theta(k_1) \Theta(-k_2). \end{aligned} \quad (41)$$

Because we have made the approximation that the transverse profile of the pump does not depend on frequency (for the frequencies of interest) in Eq. (41) we set  $\omega_{Syq} = cq_x$  in the Dirac delta function.

We now employ the nearest-neighbor tight-binding approximation [27] and expand the  $D_{Fk}^i(\mathbf{r})$  modes in terms of the single-cavity quasimodes  $N_{Fp}^i(\mathbf{r})$  as

$$D_{Fk}^i(\mathbf{r}) = \sqrt{\frac{D}{2\pi}} \sum_p N_{Fp}^i(\mathbf{r}) e^{ik_p D}, \quad (42)$$

which leads to the lossy frequency dispersion given in Eq. (1). The single-cavity quasimodes and frequencies are calculated in the standard way using finite difference time domain calculations [27]. Assuming that the cavity modes are well

localized [44], we obtain

$$\begin{aligned} \Phi(k_1, k_2) &= \frac{i\alpha D}{2\beta\hbar\sqrt{\epsilon_0\pi}} \sqrt{(\hbar\omega_F)^2 \hbar\omega_S} \int dq_x \varphi(q_x) \\ &\times \sum_p \int d\mathbf{r} \chi_2^{ijy}(\mathbf{r}) \frac{[N_{Fp}^i(\mathbf{r}) N_{Fp}^j(\mathbf{r})]^* f(y, z) e^{iq_P x}}{\epsilon_0 n^4(\mathbf{r}; \omega_F)} \\ &\times e^{-i(k_1+k_2)pD} \delta(cq_x - \omega_{Fk_1} - \omega_{Fk_2}) \Theta(k_1) \Theta(-k_2). \end{aligned} \quad (43)$$

We define

$$\varphi(q) = \sqrt{W_T / \sqrt{2\pi}} \exp \left[ -\left( \frac{(q - q_P) W_T}{2} \right)^2 \right], \quad (44)$$

and, because the spatial extent of the single-cavity quasimodes is small relative to that of the pump field, in the integral in Eq. (43) we replace  $f(y, z)$  by

$$f(y=0, z=pD) \approx \frac{\sqrt{2}}{\sqrt{\pi} W_S} e^{-\frac{p^2 D^2}{W_S^2}} \quad (45)$$

to obtain the approximate expression

$$\begin{aligned} \Phi(k_1, k_2) &= \frac{i\alpha\bar{\chi}_2}{\beta} \sqrt{\frac{\hbar\omega_F^2 \omega_S W_T}{\epsilon_0 (2\pi)^{3/2}}} e^{-\frac{(k_1+k_2)^2 W_S^2}{4}} \int dq_x e^{-\frac{(q-q_P)^2 W_T^2}{4}} \\ &\times \delta(\omega_{Sq_x} - \omega_{Fk_1} - \omega_{Fk_2}) \Theta(k_1) \Theta(-k_2), \end{aligned} \quad (46)$$

where

$$\bar{\chi}_2 \equiv \int d\mathbf{r} \chi_2^{ijy}(\mathbf{r}) \frac{[N_{F0}^i(\mathbf{r}) N_{F0}^j(\mathbf{r})]^* e^{iq_P x}}{\epsilon_0 n^4(\mathbf{r}; \omega_F)} \quad (47)$$

is the effective second-order susceptibility for the system [45] (see Appendix C for more details). Note that there are two ways in which phase matching appears in the expression for the biphoton wave function. First, it appears as the Gaussian factor containing  $W_S$  in Eq. (46), which accounts for phase matching along the waveguide. This is what provides the constraint that the wave vectors of the two photons must be of opposite sign. Second, it appears in the mode overlap in the expression for the effective susceptibility [Eq. (47)], where the factor of  $e^{iq_P x}$  will result in a degradation of the generation rate if the slab is thick relative to  $1/q_P$ . As is discussed in Refs. [16,17], one can reduce this degradation by working with a layered photonic crystal slab to provide quasiphasematching in the vertical ( $x$ ) direction. However, as this is not the focus of this work, we do not pursue this here.

For  $\omega_{Fk} \equiv \omega_F [1 - \beta_1 \cos(kD)]$ , which we consider to be a real quantity at this point, Eq. (46) can be rewritten as

$$\begin{aligned} \Phi(k_1, k_2) &= Q_0 \int dq_x e^{-\frac{(k_1+k_2)^2 W_S^2}{4}} e^{-\frac{(q-q_P)^2 W_T^2}{4}} \delta \left\{ q_x - \frac{1}{c} [\omega_{Fk_1} + \omega_{Fk_2}] \right\} \Theta(k_1) \Theta(-k_2) \\ &= Q_0 \exp \left( \frac{-(k_1+k_2)^2 W_S^2}{4} \right) \exp \left\{ -\left( \frac{2\omega_F - \beta_1 \omega_F [\cos(k_1 D) + \cos(k_2 D)] - \omega_P}{2c} \right)^2 W_T^2 \right\} \Theta(k_1) \Theta(-k_2), \end{aligned} \quad (48)$$

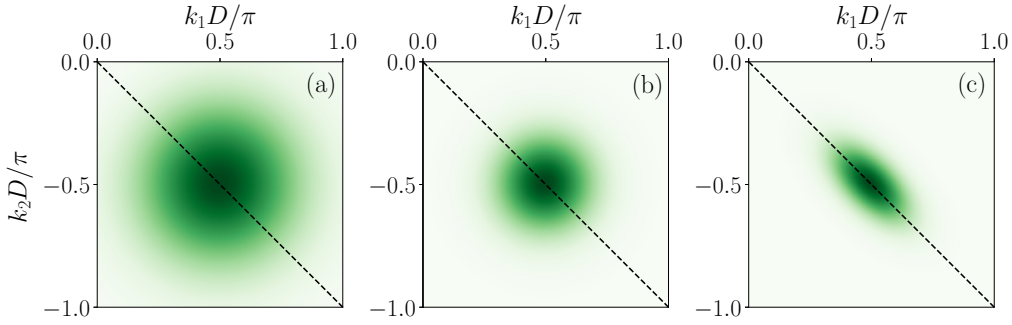


FIG. 2. Biphoton wave function of Eq. (48) for three different pumping configurations: (a)  $\sigma_+ D = \sigma_- D = 0.47$ , (b)  $\sigma_+ D = \sigma_- D = 0.28$ , and (c)  $\sigma_+ D = 0.14$ ,  $\sigma_- D = 0.28$ . In all these three cases we consider  $k_0 = \pi/2D$ .

where

$$Q_0 \equiv \frac{i\alpha \bar{\chi}_2}{\beta c} \sqrt{\frac{\hbar \omega_F^2 \omega_S W_T}{\varepsilon_0 (2\pi)^{3/2}}}. \quad (49)$$

In order to derive analytic expressions for the photon number and correlation variance as a function of cavity index  $p$ , we need to place further restrictions on the pump pulse. From the first exponential in Eq. (48), we see that the biphoton wave function will only be non-negligible if  $k_2$  is approximately equal to  $-k_1$ . Thus we set

$$k_1 \rightarrow k_0 + \delta_1, \quad k_2 \rightarrow -k_0 + \delta_2, \quad (50)$$

where the  $\delta_i$  are small relative to  $W_S$ , where  $k_0$  is determined by the central frequency of the pump, through the equation

$$\omega_p = 2\omega_{Fk_0} = 2\omega_F - 2\beta_1 \omega_F \cos(k_0 D). \quad (51)$$

In order to obtain a biphoton wave function for which there is an analytic Schmidt decomposition, we take  $k_0 = \pi/(2D)$  and choose the frequency width parameter  $W_T$  of the pulse to satisfy  $c/W_T \ll \Delta$ , where  $\Delta = 2\omega_F \beta_1$ . Now, expanding the cosines in Eq. (48) to first order in  $\delta_1$  and  $\delta_2$ , the biphoton wave function can be rewritten as

$$\begin{aligned} & \Phi(k_0 + \delta_1, -k_0 + \delta_2) \\ &= \sqrt{\frac{2}{\pi \sigma_+ \sigma_-}} \exp\left(-\frac{(\delta_1 + \delta_2)^2}{2\sigma_+^2}\right) \exp\left(-\frac{(\delta_1 - \delta_2)^2}{2\sigma_-^2}\right), \end{aligned} \quad (52)$$

where

$$\sigma_+ \equiv \frac{\sqrt{2}}{W_S} \quad (53)$$

and

$$\sigma_- \equiv \frac{\sqrt{2}c}{W_T \beta_1 \omega_F D \sin(|k_0|D)}. \quad (54)$$

Strictly speaking, the biphoton wave function of Eq. (52) does not satisfy the restriction that it is zero unless  $k_1 > 0$  and  $k_2 < 0$ . However, as long as  $\sigma_+$  and  $\sigma_-$  are chosen to be small enough, then these conditions are satisfied to a very high degree. In what follows, we shall only consider situations where this is the case. Using the normalization condition

$\int dk_1 dk_2 |\Phi(k_1, k_2)|^2 = 1$ , it can be shown that

$$Q_0 = \sqrt{\frac{2}{\pi \sigma_+ \sigma_-}}. \quad (55)$$

In Fig. 2 we plot three sample biphoton wave functions of the form given in Eq. (52) for different  $\sigma_+$  and  $\sigma_-$  for  $k_0 = \pi/2D$ .

To graphically illustrate the validity of the assumptions made to obtain Eq. (52), in Fig. 3 we plot the dispersion of our CROW. The physical parameters of the CROW are from Ref. [27]. It consists of a dielectric slab of refractive index  $n = 3.4$  having a square array of cylindrical air voids of radius  $a = 0.4d$ , height  $h = 0.8d$ , and lattice vectors  $\mathbf{a}_1 = d\hat{\mathbf{x}}$  and  $\mathbf{a}_2 = d\hat{\mathbf{y}}$ , where  $d$  is the period. The cavities are point defects formed by periodically removing air voids in a line with  $D = 2d$  (see Fig. 1). The complex frequency  $\tilde{\omega}_F$  and the complex coupling parameter  $\tilde{\beta}_1$  of the structure are  $(0.305 - i7.71 \times 10^{-6})4\pi c/D$ , and  $9.87 \times 10^{-3} - i1.97 \times 10^{-5}$ , respectively. To visualize the biphoton wave function superimposed on

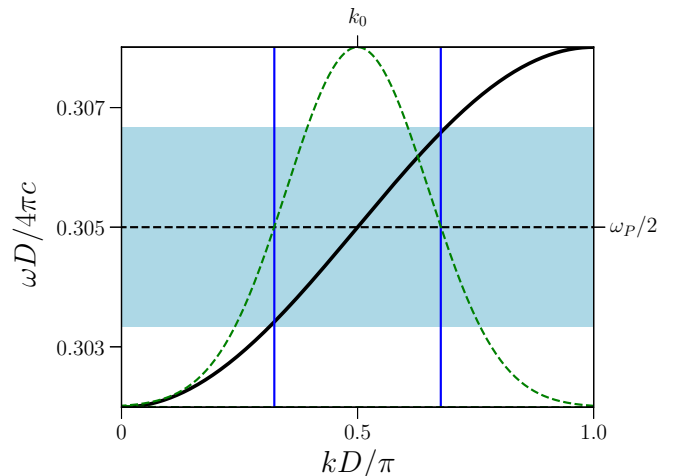


FIG. 3. The CROW dispersion relation and biphoton wave function. The solid black line shows the frequency as a function of the Bloch vector for the CROW structure. The dashed horizontal line gives the pump frequency divided by two. The dashed green line gives the function  $\Phi(k, -k)$  for  $k_0 = \pi/(2D)$ . The two vertical solid blue lines indicate the FWHM in  $k$ , while the shaded blue region indicates the FWHM in frequency, both of which can be found from Eq. (48) for  $\sigma_+ D = \sigma_- D = 0.47$ .

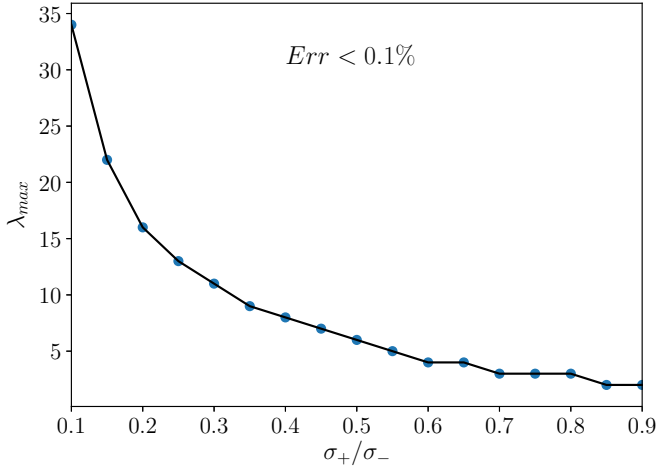


FIG. 4. Maximum number of Schmidt modes required to be considered in  $\Phi$  as a function of  $\sigma_+/\sigma_-$  to ensure  $\text{Err} < 0.1\%$ .

the CROW dispersion, we plot  $\Phi(k, -k)$  for  $W_S = 3D$  and  $\sigma_+ = \sigma_-$  in Fig. 3 as well. As can be seen, the first-order expansion of  $\cos(k_1 D)$  and  $\cos(k_2 D)$  about  $k_0$  and  $-k_0$  is accurate as the dispersion within this range is very close to linear. In order for our Schmidt decomposition to be valid for this structure,  $\sigma_+ D$  and  $\sigma_- D$  cannot be increased significantly beyond the chosen value of 0.47 otherwise the biphoton wave function will not be confined to the quadrant where  $k_1 > 0$  and  $k_2 < 0$ . Note that increasing the pump width to higher values,  $W_S > 3D$ , increases the accuracy of our approximation, as is evident from Figs. 2(b) and 2(c) where  $W_S$  is  $5.05D$  and  $10.10D$ , respectively.

Before employing a Schmidt decomposition, we present the relation between  $\sigma_{\pm}$  and the temporal and spatial full width at half maximum (FWHM) of the pump pulse. Using Eqs. (39) and (54), the temporal FWHM of the pump can be written as

$$\Delta t_{\text{FWHM}} = \frac{2\sqrt{\ln 2}\tau}{\sigma_- D}, \quad (56)$$

where  $\tau \equiv 1/\text{Re}(\tilde{\omega}_F \tilde{\beta}_1)$  is the time for a pulse with Bloch vector  $k = k_0 = \pi/(2D)$  to travel one period. Similarly, using Eqs. (44) and (53), the spatial FWHM of the pump is found to be

$$\Delta r_{\text{FWHM}} = \frac{2\sqrt{\ln 2}}{\sigma_+}. \quad (57)$$

Using these two equations, one can obtain a clear understanding of the necessary pumping conditions. For instance, the quantities considered in Fig. 2(a) correspond to a pump with  $3.54\tau$  and  $3.54D$  as the temporal and spatial

FWHM, respectively. As we show later, for our CROW, the propagation loss in the system is very small while the squeezed light is being generated, which validates the neglect of loss during the generation process.

The special form of the biphoton wave function, Eq. (52), allows us to perform a Schmidt decomposition analytically [46–48] for  $\sigma_- \geq \sigma_+$  as

$$\begin{aligned} & \sqrt{\frac{2}{\pi\sigma_+\sigma_-}} \exp\left(-\frac{(\delta_1 + \delta_2)^2}{2\sigma_+^2}\right) \exp\left(-\frac{(\delta_1 - \delta_2)^2}{2\sigma_-^2}\right) \\ &= \sum_{\lambda} \sqrt{p_{\lambda}} \psi_{\lambda}(\delta_1) \psi_{\lambda}(\delta_2), \end{aligned} \quad (58)$$

where

$$p_{\lambda} = 4\sigma_+\sigma_- \frac{(\sigma_+ - \sigma_-)^{2\lambda}}{(\sigma_+ + \sigma_-)^{2(\lambda+1)}}, \quad (59)$$

$$\begin{aligned} \psi_{\lambda}(\delta) &= (-i)^{\lambda} \sqrt{\frac{\sqrt{2}}{2^{\lambda}\lambda! \sqrt{\pi\sigma_+\sigma_-}}} \\ &\times \exp\left(-\frac{\delta^2}{\sigma_+\sigma_-}\right) H_{\lambda}\left(\frac{\sqrt{2}\delta}{\sqrt{\sigma_+\sigma_-}}\right), \end{aligned} \quad (60)$$

and the  $H_{\lambda}(x)$  are Hermite polynomials of order  $\lambda$ . Note that the Schmidt number is given by [49]

$$K = \frac{1}{\sum_{\lambda} p_{\lambda}} = \frac{\sigma_+^2 + \sigma_-^2}{2\sigma_+\sigma_-}. \quad (61)$$

Using Eq. (59) for the special case where  $\sigma_- = \sigma_+ = \sigma$ , it can be shown that the only nonzero term in Eq. (64) is for  $\lambda = 0$ . However, in general, one needs to include several of the Schmidt modes (up to  $\lambda = \lambda_{\max}$ ) to accurately represent the biphoton wave function. To quantify the accuracy of the Schmidt decomposition used in our calculations, we define an error function as

$$\text{Err} = \sqrt{\frac{\int dk_1 dk_2 |\Phi(k_1, k_2) - \Phi_{\text{App}}(k_1, k_2)|^2}{\int dk_1 dk_2 |\Phi(k_1, k_2)|^2}}, \quad (62)$$

where  $\Phi$  and  $\Phi_{\text{App}}$  are the exact and approximate expressions, respectively, given by Eq. (52) and

$$\Phi_{\text{App}}(k_0 + \delta_1, -k_0 + \delta_2) = \sum_{\lambda=0}^{\lambda_{\max}} \sqrt{p_{\lambda}} \psi_{\lambda}(\delta_1) \psi_{\lambda}(\delta_2). \quad (63)$$

In Fig. 4 we plot the index of the maximum Schmidt mode needed to be included in  $\Phi_{\text{App}}$ , in order to ensure  $\text{Err} < 0.1\%$ . For example, as can be seen, when  $\sigma_- = 2\sigma_+$ , one needs to include six terms ( $\lambda_{\max} = 6$ ) to achieve the desired accuracy.

Using these results in Eqs. (26) and (31), the time-dependent average photon number in the  $p$ th cavity is found to be

$$\langle \hat{a}_p^{\dagger}(t) \hat{a}_p(t) \rangle = \frac{D}{2\pi} e^{-2\text{Re}\{i\tilde{\omega}_F [1 - \tilde{\beta}_1 \cos(|k_0|D)]t\}} \sum_{\lambda} \sinh^2(r_{\lambda}) \frac{\sqrt{2\sigma_+\sigma_-\pi}}{2^{\lambda}\lambda!} \left( |H_{\lambda}(\tilde{S}_{p-})|^2 e^{-\frac{(\tilde{S}_{p-}^2 + \tilde{S}_{p-}^2)}{2}} + |H_{\lambda}(\tilde{S}_{p+})|^2 e^{-\frac{(\tilde{S}_{p+}^2 + \tilde{S}_{p+}^2)}{2}} \right), \quad (64)$$

where

$$\tilde{S}_{p\pm} = (\tilde{\omega}_F \tilde{\beta}_1 D \sin(|k_0|D)t \pm pD) \sqrt{\frac{\sigma_+\sigma_-}{2}}. \quad (65)$$

The time-dependent average photon number in the  $p$ th cavity when  $\sigma_+ = \sigma_-$  can be simplified to

$$\langle \hat{a}_p^\dagger(t) \hat{a}_p(t) \rangle = \frac{\sigma D}{\sqrt{2\pi}} e^{-2\text{Re}\{i\tilde{\omega}_F[1-\tilde{\beta}_1 \cos(|k_0|D)]t\}} \sinh^2(r_0) \left( e^{-\left(\frac{\tilde{\sigma}_{p+}^2 + \tilde{\sigma}_{p-}^2}{2}\right)} + e^{-\left(\frac{\tilde{\sigma}_{p+}^2 + \tilde{\sigma}_{p-}^2}{2}\right)} \right). \quad (66)$$

We note that using Eq. (66) for a lossless system, one finds that the total number of photons in the CROW is  $2 \sinh^2(r_0)$ , independent of  $\sigma$ , which agrees with the total number of generated photons in any two-mode squeezed state.

Following a procedure similar to that used to arrive at Eq. (64), one can derive the following expectation value for  $\langle \hat{a}_p(t) \hat{a}_{p'}(t) \rangle$ , which is needed in Eq. (34) to evaluate the variances of the quadrature operators and the correlation variance in the CROW structure:

$$\begin{aligned} \langle \hat{a}_p(t) \hat{a}_{p'}(t) \rangle &= \frac{D}{2\pi} \sum_{\lambda} (-1)^{\lambda} [\cosh(r_{\lambda}) \sinh(r_{\lambda})] e^{-i2\tilde{\omega}_F[1-\tilde{\beta}_1 \cos(|k_0|D)]t} \frac{\sqrt{2\sigma_+ \sigma_- \pi}}{2^{\lambda} \lambda!} \\ &\times \left[ e^{-i|k_0|(p-p')D} H_{\lambda}(\tilde{\mathcal{S}}_{p+}) H_{\lambda}(\tilde{\mathcal{S}}_{p'-}) e^{-\left(\frac{\tilde{\sigma}_{p+}^2 + \tilde{\sigma}_{p'-}^2}{2}\right)} + e^{i|k_0|(p-p')D} H_{\lambda}(\tilde{\mathcal{S}}_{p-}) H_{\lambda}(\tilde{\mathcal{S}}_{p'+}) e^{-\left(\frac{\tilde{\sigma}_{p-}^2 + \tilde{\sigma}_{p'+}^2}{2}\right)} \right]. \end{aligned} \quad (67)$$

Note that  $\langle \hat{a}_p^\dagger(t) \hat{a}_{p'}^\dagger(t) \rangle$  is simply the complex conjugate of Eq. (67).

In the next section we will use these equations to determine the photon number and correlation variance under a variety of different pump conditions.

#### IV. RESULTS

Using the expectation values derived in Sec. III, we can now study the photon evolution and inseparability criteria for the generalized two-mode squeezed light inside the CROW structure. In Fig. 5 we plot the average number of photons in the  $p$ th cavity for  $p = 0, 40$  as a function of time for both a lossy (solid green line) and lossless (dashed gray line) system. The propagation of light between the coupled cavities and ef-

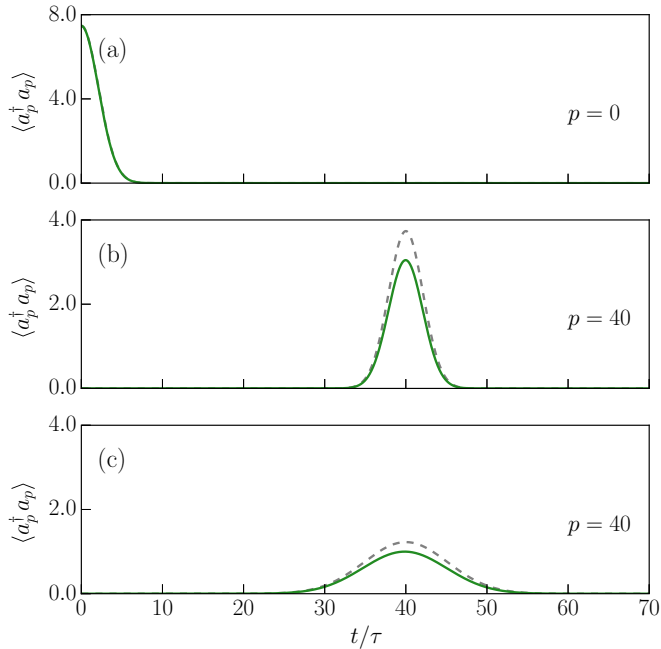


FIG. 5. Average photon number in the (a) central and (b) 40th cavities of the CROW as a function of time for  $\sigma_+ D = \sigma_- D = 0.47$  and  $\beta = 2.2$ . (c) The time-dependent average photon number for  $\sigma_+ D = 0.14$ ,  $\sigma_- D = 0.28$ , and  $\beta = 2.2$ . The dashed gray lines show the case in which the effect of loss is ignored.

fect of loss on the number of photons in each cavity is evident in Figs. 5(a) and 5(b), where  $\sigma_+ D = \sigma_- D = 0.47$ . Because the system and pump are spatially symmetric, the results are identical for  $p \rightarrow -p$ . In Fig. 5(c) we plot the time-dependent average photon number in the 40th cavity with  $\beta = 2.2$  still, but with the  $\sigma_+ D = 0.14$  and  $\sigma_- D = 0.28$ . As can be seen, the pulse width is wider for this smaller  $\sigma_+$ , as expected.

Since our input pump state is a coherent state, the number of pump photons is  $N_p = |\alpha|^2$ . We now examine what the pump parameters will be for a specific case of interest. We again consider the case where  $\sigma_+ D = \sigma_- D = 0.47$ ; using Eqs. (56) and (57) this gives temporal and spatial FWHM for the pump of 295 fs and 3.3  $\mu\text{m}$ , respectively. We choose the CROW material to be  $\text{Al}_{0.35}\text{Ga}_{0.65}\text{As}$  due to its high nonlinearity and relatively large band gap. In addition, we choose the pump wavelength to be  $\lambda_S = 775$  nm, which not only results in generating counterpropagating signal and idler photons at the telecommunication wavelength  $\lambda_F = 1550$  nm, but also ensures operation below the band gap of  $\text{Al}_{0.35}\text{Ga}_{0.65}\text{As}$ . Choosing the periodicity of the CROW structure to yield a signal central wavelength of 1550 nm, gives  $D \approx 0.9$   $\mu\text{m}$ . Using Eq. (47) and the normalization condition given in Appendix A,  $\tilde{\chi}_2$  for our structure is approximately given by  $\tilde{\chi}_2 \approx \chi_2/n^2(\omega_F)$ , where  $\chi_2 \approx 100$  pm/V, appropriate for AlGaAs alloys [12,50,51], and  $n \approx 3.4$  at  $\omega_F$ . We now seek to determine the approximate number of pump photons under the above conditions that will give a squeezing parameter of 2.2. Employing Eqs. (49) and (55), the average number of photons in the pump is found to be  $7.4 \times 10^{10}$ , which gives a total pump pulse energy of approximately 19 nJ. We note that all of the above pump characteristics are easily achievable from a Ti:sapphire laser.

In Fig. 6 we plot the time-dependent correlation variances for different sets of lossy and lossless cavities in blue and gray, respectively. Note that there are fast oscillations that are not observable on this timescale. The dashed lines in the insets show the inseparability criteria below which the light is considered to be entangled. Here we only focus on cases where the two cavities considered are located the same distance from the central cavity, as this will yield the maximum entanglement; however, using Eq. (34) one can explore the entanglement between any two cavities of the CROW. As can be seen in Figs. 6(a) and 6(b), due to the loss in the system, the degree of entanglement decreases as the system evolves in

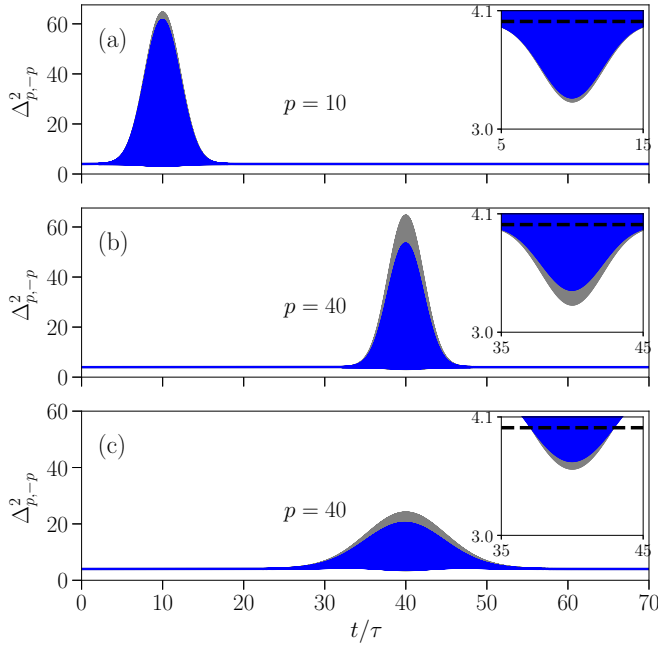


FIG. 6. (a) and (b) Correlation variance between different pairs of cavities in the CROW as a function of time for  $\sigma_+ D = \sigma_- D = 0.47$  and  $\beta = 2.2$ . (c) The time-dependent correlation variance for  $\sigma_+ D = 0.14$ ,  $\sigma_- D = 0.28$ , and  $\beta = 2.2$ . The results for a lossless system are shown in gray.

time, whereas for a lossless system (the gray color) the degree of entanglement does not change as the light propagates.

In Fig. 7 we plot the maximum number of photons for a lossless and lossy CROW as a function of the cavity index  $p$ . As expected, when loss is included, the number of photons decreases as we move away from the central cavity. In Fig. 7 we also plot the minimum correlation variance for the lossless and lossy CROW as a function of cavity index  $p$ . As can be

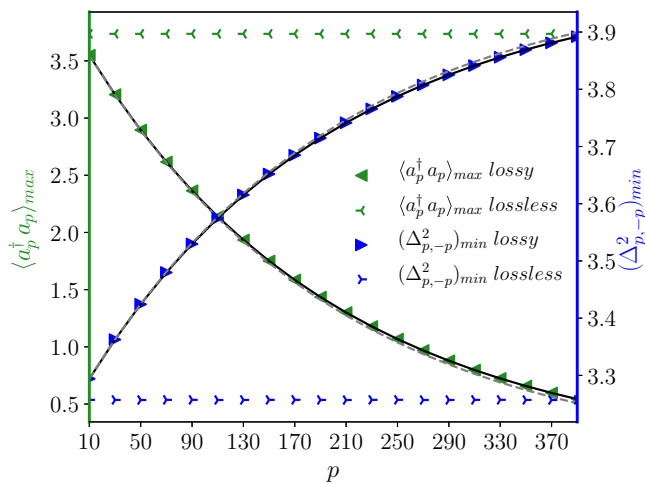


FIG. 7. Maximum number of photons (left axis) as a function of the cavity index and minimum correlation variances (right axis) between different symmetrically displaced pairs of cavities for  $\sigma_+ D = \sigma_- D = 0.47$  and  $\beta = 2.2$ . The solid black and dashed gray lines represent the results from Eqs. (69) and (70) with and without including  $\exp[(V_I t_{\max})^2 \frac{\sigma^2}{2}]$ , respectively.

seen, due to the reduction in the number of photons in the lossy case, there is a decrease in the degree of entanglement as a function of  $p$ . For instance, the minimum correlation variance at the tenth cavity is 0.9 times the corresponding value at the 100th cavity.

For a general pump, the evolution equations for the photon number and correlation variance are quite complicated and it is difficult to discern the general behavior or the effects of loss from the full equations. However, for the special case where  $\sigma_+ = \sigma_- = \sigma$  and  $k_0 = \pi/2D$ , approximate analytic expressions can be obtained. We begin by defining the complex quantity  $\tilde{V} = V_R + iV_I = \tilde{\omega}_F \beta_1 D$ , which enables us to rewrite  $\tilde{S}_{p\pm}^2$  as

$$\begin{aligned} \tilde{S}_{p\pm}^2 &= [(V_R + iV_I)t \pm pD]^2 \frac{\sigma^2}{2} \\ &= [(V_{Rt} \pm pD)^2 + 2i(V_{Rt} \pm pD)V_{It} - (V_{It})^2] \frac{\sigma^2}{2}. \end{aligned} \quad (68)$$

Considering only the dominant terms in Eq. (66), to a very good approximation one can show that the time at which the photon number in the  $p$ th cavity peaks in a lossless system is  $t_{\max} = p\tau \approx p/\omega_F \beta_1$ . As can be seen in Fig. 5, the photon number peaks at essentially the same time in both lossy and lossless system. Using  $t_{\max}$ , we are able to derive the following approximate expression for the maximum photon number in the  $p$ th cavity (for  $p > 0$ ) in a lossy system:

$$\langle a_p^\dagger a_p \rangle_{\max} \approx \frac{\sigma D}{\sqrt{2\pi}} \sinh^2(r_0) e^{-2\nu_F p\tau} e^{(V_I p\tau)^2 \frac{\sigma^2}{2}}. \quad (69)$$

Following the same procedure and using Eqs. (34) and (67), one obtains

$$\begin{aligned} (\Delta^2_{p,-p})_{\min} &\approx 4 + 4 \frac{\sigma D}{\sqrt{2\pi}} [2 \sinh^2(r_0) - \sinh(2r_0)] \\ &\quad \times e^{-2\nu_F p\tau} e^{(V_I p\tau)^2 \frac{\sigma^2}{2}}. \end{aligned} \quad (70)$$

We note first that both the photon number and the deviation of the correlation variance from 4 depend linearly on  $\sigma$ . Thus, as expected, the separability is largest when the pump is short in time and narrow in space (for a fixed squeezing parameter  $r_0$ ). Now, according to Eqs. (69) and (70), under the above-mentioned pumping conditions the effect of loss on the maximum number of photons and on the entanglement as a function of  $p$  is given by two exponential factors. The first factor accounts for the intrinsic loss in an individual cavity (which is also the intrinsic loss of the Bloch mode with  $k = \pi/2D$ ). The second factor accounts for the loss dispersion in the CROW, and results in a reduction in the loss. Of course, these analytic results are only valid when the effect of the dispersion of the loss is small.

We now consider how well these approximate expressions reproduce the exact results. In Fig. 7 we plot the results of Eqs. (69) and (70) with (black solid line) and without (red solid line) including the factor  $\exp[(V_I p\tau)^2 \frac{\sigma^2}{2}]$ . As can be seen, for this CROW the full approximate analytic expressions very accurately reproduces the exact results. Moreover, to a very good approximation, one can evaluate Eqs. (69) and (70) neglecting the loss-dispersion factor  $\exp[(V_I p\tau)^2 \frac{\sigma^2}{2}]$ . For example, for  $\sigma_- D = \sigma_+ D = 0.47$  and  $p = 350$ , the first and

TABLE I. The maximum number of photons and the deviation of the minimum of the correlation variance from the inseparability threshold of 4 in a lossless system for  $\beta = 2.2$  and different pumping configurations.

$\sigma_- D$	0.28	0.28	0.47	0.47	0.47
$\sigma_+ D$	0.14	0.28	0.12	0.28	0.47
$\langle a_p^\dagger a_p \rangle_{\max}$	1.23	2.24	0.77	2.51	3.74
$4 - (\Delta_{p,-p}^2)_{\min}$	0.38	0.44	0.58	0.65	0.74

the second exponential factors in Eqs. (69) and (70) are 0.18 and 1.10, respectively, showing that loss dispersion only changes the results by 10%. In general, it can be shown that in order to have less than 10% error in evaluating the photon number and the difference of the correlation variance from 4, the range of  $p$  must be limited to  $p \leq \sqrt{2}/(10V_I \tau \sigma)$ .

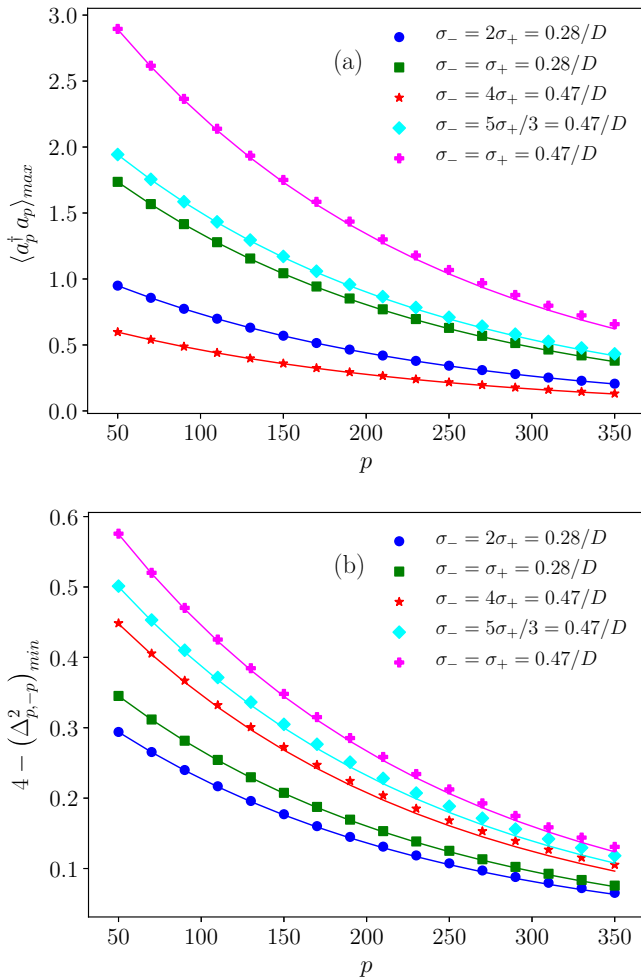


FIG. 8. (a) Maximum number of photons and (b) the deviation of the minimum of the correlation variance from the inseparability threshold of 4 for a lossy system and selected range of cavities for  $\beta = 2.2$  and different pumping configurations. The solid lines represent the results from data given in Table I and the exponential factor  $\exp(-2\gamma_F p \tau)$ , and the markers show the results from the full calculations.

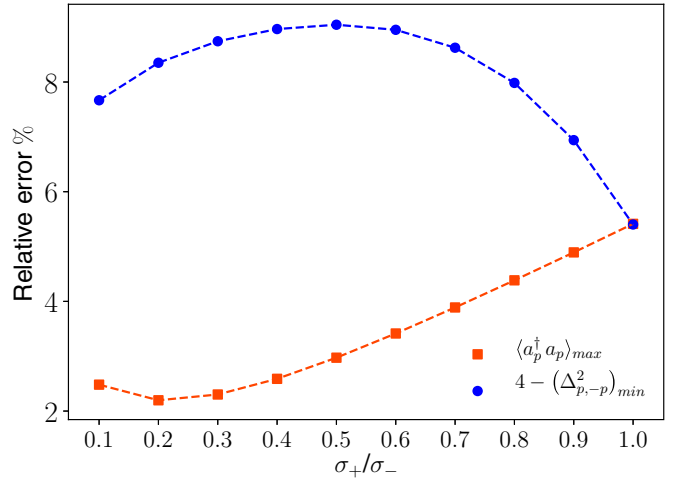


FIG. 9. Relative deviation of the results by the exponential factor  $\exp(-2\gamma_F p \tau)$  from the results of the full calculation as a function of  $\sigma_+/\sigma_-$  for  $p = 350$  and  $\sigma_- D = 0.47$ .

Finally, we now consider the more general cases in which  $\sigma_-$  is not necessarily equal to  $\sigma_+$ . Under these conditions, we cannot derive simple expressions for the maximum photon number and entanglement as a function of  $p$ . We present the results of the full calculations for a *lossless* system in Table I for a number of different pump durations and spatial widths; all other parameters are the same as in the previous plots. As can be seen, the maximum entanglement is obtained when the pump duration is as short as possible and the pump width is as narrow as possible (i.e.,  $\sigma_+ D = \sigma_- D = 0.47$  for our system).

We have also performed full calculations for the evolution in the presence of loss for different pump configurations. In Fig. 8 we compare the results of the full calculations with the results when the loss is incorporated approximately using only the exponential factor  $\exp(-2\gamma_F p \tau)$ . We plot the maximum number of photons and the deviation of the minimum of the correlation variance from the inseparability threshold of 4 for a lossy system as a function of  $p$  for different pumping configurations. As can be seen, for short distances from the central cavity (small  $p$ ), the effect of loss on the result can, to a very good approximation, still be explained by only including the exponential factor  $\exp(-2\gamma_F p \tau)$ . However, for the cavities far from the central cavity (large  $p$ ), although the general trends can still be predicted by such an approximation, the difference between the exact and approximation results becomes pronounced and the validity of this approximation becomes questionable. In order to show the difference between exact and approximate results for large  $p$ , in Fig. 9 we plot the relative difference between the results from the full calculations and those from approximating the loss in the system by only considering the exponential factor  $\exp(-2\gamma_F p \tau)$  as a function of  $\sigma_+/\sigma_-$ , for  $p = 350$  and  $\sigma_- D = 0.47$ . As expected, when  $\sigma_+ = \sigma_-$ , we obtain a relative error of approximately 5.4%, which is simply due to the dispersion factor  $\exp[(V_I p \tau)^2 \sigma_-^2]$ . However, in general, the error depends on  $\sigma_+/\sigma_-$ , and is different for the photon number and correlation variance, due to the different way in which loss dispersion affects these two quantities. As can be seen in this specific example, evaluating

$4 - (\Delta_{p,-p}^2)_{\min}$  using the approximation method results in a 9% deviation from the results of the full calculations when  $\sigma_+ = 0.5\sigma_-$ , while the relative difference for the maximum number of photons is always less than 5.4%. It is thus evident that a simple exponential factor will capture the general effect of loss on the correlation, but it may not be very accurate depending on the structure and the pump conditions.

## V. CONCLUSION

In this work we studied the generation and propagation of entangled states in lossy coupled-cavity systems. We applied the tight-binding method to evaluate the fields and complex frequencies for the leaky modes of lossy coupled-cavity system, and presented analytic time-dependent expressions for the photon number and correlation variance in a lossy CROW structure. We showed how properties such as the average number of photons in each cavity and the correlations between cavities are affected by loss. For the CROW structure considered in this work, we found that as the light gets far from the central cavity, the effects of loss become more significant and cannot be ignored. Moreover, we obtained simple, approximate analytic expressions for the effects of loss on the propagation of the generated light in the CROW, and have shown that they can be used to predict general trends. However, depending on the details of the pumping conditions and the CROW structure itself, the accuracy of this approximation varies, and to get an accurate result, specifically for cavities far from the central cavity, the effect of loss cannot be well described using a simple exponential factor that is given by the loss in an individual cavity. Using full numerical results is suggested for optimization. Yet these analytic results allow researchers to easily explore the spectral and spatial pumping configurations needed to generate the counterpropagating entangled states in a CROW.

## ACKNOWLEDGMENTS

This work was supported by Queen's University and the Natural Sciences and Engineering Research Council of Canada (NSERC).

## APPENDIX A

In this Appendix we present the normalization condition for the modes. Considering the refractive index of the material to be nondispersive within the range of frequency considered here, following Yang *et al.* [32], the normalization conditions can be written as

$$\int d\mathbf{r} \frac{\mathbf{D}_{Fk}^*(\mathbf{r}) \cdot \mathbf{D}_{Fk'}(\mathbf{r})}{\epsilon_0 n^2(\mathbf{r}; \omega_F)} = \delta(k - k') \quad (\text{A1})$$

and

$$\int d\mathbf{r} \frac{\mathbf{M}_{Smq}^*(\mathbf{r}) \cdot \mathbf{M}_{Smq'}(\mathbf{r})}{\epsilon_0 n^2(\mathbf{r}; \omega_{Sm})} = \delta_{mm'} \delta(\mathbf{q} - \mathbf{q}'). \quad (\text{A2})$$

Using Eq. (42) in Eq. (A1) we obtain the normalization condition for the single-cavity modes as

$$\int d\mathbf{r} \frac{N_{Fp}^*(\mathbf{r}) \cdot N_{Fp'}(\mathbf{r})}{\epsilon_0 n^2(\mathbf{r}; \omega_F)} = \delta_{pp'}. \quad (\text{A3})$$

## APPENDIX B

In this Appendix we provide a road map on how to evaluate the CV inseparability criterion of Mancini *et al.* ( $\overline{\Delta}_{p,p'}^2 < 4$ ) in our system and then compare it with our results obtained using the criterion of Duan *et al.* ( $\Delta_{p,p'}^2 < 4$ ).

Rewriting the variances within  $\overline{\Delta}_{p,p'}^2 < 4$  [Eq. (35)] in terms of creation and annihilation operators, we find that its evaluation requires analytic expressions for  $\langle \hat{a}_p^\dagger(t) \hat{a}_p(t) \rangle$ ,  $\langle \hat{a}_{p'}^\dagger(t) \hat{a}_{p'}(t) \rangle$ ,  $\langle \hat{a}_p(t) \hat{a}_{p'}(t) \rangle$ ,  $\langle \hat{a}_p^\dagger(t) \hat{a}_{p'}^\dagger(t) \rangle$ , and  $\langle \hat{a}_p^\dagger(t) \hat{a}_{p'}(t) \rangle$ , only the last of which was not evaluated in the main text. Following a procedure similar to that used in deriving Eqs. (64) and (67), we obtain

$$\begin{aligned} & \langle a_p^\dagger(t) a_{p'}(t) \rangle \\ &= \frac{D}{2\pi} e^{-2\text{Re}(i\tilde{\omega}_0[1-\tilde{\beta}_1 \cos(|k_0|D)]t)} \sum_{\lambda} \sinh^2(r_{\lambda}) \frac{\sqrt{2\sigma_+ \sigma_- \pi}}{2^{\lambda} \lambda!} \\ & \times \left[ e^{i|k_0|(p-p')D} H_{\lambda}(\tilde{S}_{p+}^*) H_{\lambda}(\tilde{S}_{p'+}) e^{-\left(\frac{\tilde{S}_{p+}^2 + \tilde{S}_{p'+}^2}{2}\right)} \right. \\ & \left. + e^{-i|k_0|(p-p')D} H_{\lambda}(\tilde{S}_{p-}^*) H_{\lambda}(\tilde{S}_{p'-}) e^{-\left(\frac{\tilde{S}_{p-}^2 + \tilde{S}_{p'-}^2}{2}\right)} \right]. \quad (\text{B1}) \end{aligned}$$

Using this expression, we calculate Mancini's correlation variance and compare it to Duan's for the configuration given in Fig. 6(b). Comparing the time intervals over which the inseparability criteria are met  $[\Delta(t/\tau)_{\text{Ent}}]$ , we find that the time intervals are identical  $[\Delta(t/\tau)_{\text{Ent}} = 37.24]$  in both cases. In addition, we find that the temporal FWHM of the deviation of  $\overline{\Delta}_{p,p'}^2$  and  $\Delta_{p,p'}^2$  from 4 are  $5.12\tau$  and  $4.96\tau$ , respectively. The very slight difference between the results indicates that there is no particular advantage to employing Mancini's criterion. Thus, in this work, we only use the criterion of Duan *et al.* since it provides more straightforward analytical expressions and is slightly less computationally intensive.

## APPENDIX C

In this Appendix we present an accurate approximate analytic result for the summation in Eq. (43). Starting from Eq. (43) we have

$$S = \sum_p e^{-\frac{p^2 D^2}{w_S^2}} e^{-ip(k_1+k_2)D}. \quad (\text{C1})$$

Approximating this sum as an integral, we obtain

$$S \approx \int dp e^{-\frac{p^2 D^2}{w_S^2}} e^{-ip(k_1+k_2)D} = \frac{1}{D} \int dp' e^{-\frac{p'^2}{w_S^2}} e^{-i2\pi p' k'}, \quad (\text{C2})$$

where  $p' = pD$  and  $k' = \frac{k_1+k_2}{2\pi}$ . Now using

$$\int_{-\infty}^{\infty} e^{-ax^2} e^{-2\pi ikx} dx = \sqrt{\frac{\pi}{a}} e^{-\frac{\pi^2 k^2}{a}}, \quad (\text{C3})$$

we can write

$$S = \frac{W_S \sqrt{\pi}}{D} \exp \left[ -\left( \frac{(k_1+k_2)W_S}{2} \right)^2 \right]. \quad (\text{C4})$$

One can show numerically that for  $W_S \geq 2D$ , the approximation made here is accurate to within 0.01%.

- [1] D. Bouwmeester, J.-W. Pan, K. Mattle, M. Eibl, H. Weinfurter, and A. Zeilinger, Experimental quantum teleportation, *Nature* **390**, 575 (1997).
- [2] T. Jennewein, G. Weihs, J.-W. Pan, and A. Zeilinger, Experimental Nonlocality Proof of Quantum Teleportation and Entanglement Swapping, *Phys. Rev. Lett.* **88**, 017903 (2001).
- [3] N. J. Cerf, N. J. Cerf, G. Leuchs, and E. S. Polzik, *Quantum Information with Continuous Variables of Atoms and Light* (Imperial College Press, London, 2007).
- [4] D. Bouwmeester, A. K. Ekert, and A. Zeilinger, *The Physics of Quantum Information: Quantum Cryptography, Quantum Teleportation, Quantum Computation* (Springer, Berlin, 2013).
- [5] D. Huang, P. Huang, D. Lin, and G. Zeng, Long-distance continuous-variable quantum key distribution by controlling excess noise, *Sci. Rep.* **6**, 19201 (2016).
- [6] A. Leverrier and P. Grangier, Continuous-variable quantum-key-distribution protocols with a non-Gaussian modulation, *Phys. Rev. A* **83**, 042312 (2011).
- [7] D. B. S. Soh, C. Brif, P. J. Coles, N. Lütkenhaus, R. M. Camacho, J. Urayama, and M. Sarovar, Self-Referenced Continuous-Variable Quantum Key Distribution Protocol, *Phys. Rev. X* **5**, 041010 (2015).
- [8] X. Jia, X. Su, Q. Pan, J. Gao, C. Xie, and K. Peng, Experimental Demonstration of Unconditional Entanglement Swapping for Continuous Variables, *Phys. Rev. Lett.* **93**, 250503 (2004).
- [9] Y. Miwa, J.-I. Yoshikawa, P. van Loock, and A. Furusawa, Demonstration of a universal one-way quantum quadratic phase gate, *Phys. Rev. A* **80**, 050303(R) (2009).
- [10] A. B. U'Ren, R. K. Erdmann, M. de la Cruz-Gutierrez, and I. A. Walmsley, Generation of Two-Photon States with an Arbitrary Degree of Entanglement Via Nonlinear Crystal Superlattices, *Phys. Rev. Lett.* **97**, 223602 (2006).
- [11] L. Sciscione, M. Centini, C. Sibilìa, M. Bertolotti, and M. Scalora, Entangled, guided photon generation in (1 + 1)-dimensional photonic crystals, *Phys. Rev. A* **74**, 013815 (2006).
- [12] Z. Yang and J. E. Sipe, Generating entangled photons via enhanced spontaneous parametric downconversion in AlGaAs microring resonators, *Opt. Lett.* **32**, 3296 (2007).
- [13] H.-T. Tan, W.-M. Zhang, and G.-x. Li, Entangling two distant nanocavities via a waveguide, *Phys. Rev. A* **83**, 062310 (2011).
- [14] H.-N. Xiong, W.-M. Zhang, X. Wang, and M.-H. Wu, Exact non-Markovian cavity dynamics strongly coupled to a reservoir, *Phys. Rev. A* **82**, 012105 (2010).
- [15] H.-T. Tan and W.-M. Zhang, Non-Markovian dynamics of an open quantum system with initial system-reservoir correlations: A nanocavity coupled to a coupled-resonator optical waveguide, *Phys. Rev. A* **83**, 032102 (2011).
- [16] X. Caillet, V. Berger, G. Leo, and S. Ducci, A semiconductor source of counterpropagating twin photons: A versatile device allowing the control of the two-photon state, *J. Mod. Opt.* **56**, 232 (2009).
- [17] A. Orioux, X. Caillet, A. Lemaître, P. Filloux, I. Favero, G. Leo, and S. Ducci, Efficient parametric generation of counterpropagating two-photon states, *J. Opt. Soc. Am. B* **28**, 45 (2011).
- [18] A. Yarov, Y. Xu, R. K. Lee, and A. Scherer, Coupled-resonator optical waveguide: A proposal and analysis, *Opt. Lett.* **24**, 711 (1999).
- [19] R. E. Slusher, L. W. Hollberg, B. Yurke, J. C. Mertz, and J. F. Valley, Observation of Squeezed States Generated by Four-Wave Mixing in an Optical Cavity, *Phys. Rev. Lett.* **55**, 2409 (1985).
- [20] M. Jasperse, L. D. Turner, and R. E. Scholten, Relative intensity squeezing by four-wave mixing with loss: An analytic model and experimental diagnostic, *Opt. Express* **19**, 3765 (2011).
- [21] H. Seifoory, S. Doutre, M. M. Dignam, and J. E. Sipe, Squeezed thermal states: The result of parametric down conversion in lossy cavities, *J. Opt. Soc. Am. B* **34**, 1587 (2017).
- [22] H. Seifoory and M. M. Dignam, Squeezed-state evolution and entanglement in lossy coupled-resonator optical waveguides, *Phys. Rev. A* **97**, 023840 (2018).
- [23] A. Rai and D. G. Angelakis, Dynamics of nonclassical light in integrated nonlinear waveguide arrays and generation of robust continuous-variable entanglement, *Phys. Rev. A* **85**, 052330 (2012).
- [24] Z. D. Walton, M. C. Booth, A. V. Sergienko, B. E. A. Saleh, and M. C. Teich, Controllable frequency entanglement via auto-phase-matched spontaneous parametric down-conversion, *Phys. Rev. A* **67**, 053810 (2003).
- [25] Z. D. Walton, A. V. Sergienko, B. E. A. Saleh, and M. C. Teich, Generation of polarization-entangled photon pairs with arbitrary joint spectrum, *Phys. Rev. A* **70**, 052317 (2004).
- [26] N. W. Ashcroft and N. D. Mermin, *Solid State Physics* (Cengage Learning, Stamford, CT, 2011).
- [27] D. P. Fussell and M. M. Dignam, Engineering the quality factors of coupled-cavity modes in photonic crystal slabs, *Appl. Phys. Lett.* **90**, 183121 (2007).
- [28] Throughout this work we place a tilde on top of quantities that are inherently complex (as opposed to real).
- [29] M. Kamandar Dezfouli, Quantum Nonlinear Optics in Lossy Coupled-Cavities in Photonic Crystal Slabs, Ph.D. thesis, Queen's University, 2015.
- [30] D. P. Fussell and M. M. Dignam, Spontaneous emission in coupled microcavity-waveguide structures at the band edge, *Opt. Lett.* **32**, 1527 (2007).
- [31] S. Saravi, T. Pertsch, and F. Setzpfandt, Generation of Counterpropagating Path-Entangled Photon Pairs in a Single Periodic Waveguide, *Phys. Rev. Lett.* **118**, 183603 (2017).
- [32] Z. Yang, M. Liscidini, and J. E. Sipe, Spontaneous parametric down-conversion in waveguides: A backward Heisenberg picture approach, *Phys. Rev. A* **77**, 033808 (2008).
- [33] A. Peres, *Quantum Theory: Concepts and Methods*, Fundamental Theories of Physics (Springer, Netherlands, 2006).
- [34] A. Ekert and P. L. Knight, Entangled quantum systems and the Schmidt decomposition, *Am. J. Phys.* **63**, 415 (1995).
- [35] H. P. Breuer and F. Petruccione, *The Theory of Open Quantum Systems* (Oxford University Press, Oxford, 2007).
- [36] M. M. Dignam and M. K. Dezfouli, Photon-quantum-dot dynamics in coupled-cavity photonic crystal slabs, *Phys. Rev. A* **85**, 013809 (2012).
- [37] L.-M. Duan, G. Giedke, J. I. Cirac, and P. Zoller, Inseparability Criterion for Continuous Variable Systems, *Phys. Rev. Lett.* **84**, 2722 (2000).
- [38] R. Simon, Peres-Horodecki Separability Criterion for Continuous Variable Systems, *Phys. Rev. Lett.* **84**, 2726 (2000).
- [39] G. Masada, K. Miyata, A. Politi, T. Hashimoto, J. L. O'Brien, and A. Furusawa, Continuous-variable entanglement on a chip, *Nat Photon* **9**, 316 (2015).

- [40] Y. Zhang, R. Okubo, M. Hirano, Y. Eto, and T. Hirano, Experimental realization of spatially separated entanglement with continuous variables using laser pulse trains, *Sci. Rep.* **5**, 13029 (2015).
- [41] S. Mancini, V. Giovannetti, D. Vitali, and P. Tombesi, Entangling Macroscopic Oscillators Exploiting Radiation Pressure, *Phys. Rev. Lett.* **88**, 120401 (2002).
- [42] M. G. Raymer, A. C. Funk, B. C. Sanders, and H. de Guise, Separability criterion for separate quantum systems, *Phys. Rev. A* **67**, 052104 (2003).
- [43] M. Hillery and M. S. Zubairy, Entanglement Conditions for Two-Mode States, *Phys. Rev. Lett.* **96**, 050503 (2006).
- [44] By well-localized we mean that the integral would be negligible unless both of these modes are at the same  $p$ .
- [45] For the range of pump frequency considered in this paper, to a very good approximation one can consider  $e^{iq_s x} \simeq e^{iq_p x}$ .
- [46] A. B. U'Ren, K. Banaszek, and I. A. Walmsley, Photon engineering for quantum information processing, *Quantum Info. Comput.* **3**, 480 (2003).
- [47] A. I. Lvovsky, W. Wasilewski, and K. Banaszek, Decomposing a pulsed optical parametric amplifier into independent squeezers, *J. Mod. Opt.* **54**, 721 (2007).
- [48] D. R. Blay, M. J. Steel, and L. G. Helt, Effects of filtering on the purity of heralded single photons from parametric sources, *Phys. Rev. A* **96**, 053842 (2017).
- [49] S. V. Zhukovsky, L. G. Helt, P. Abolghasem, D. Kang, J. E. Sipe, and A. S. Helmy, Bragg reflection waveguides as integrated sources of entangled photon pairs, *J. Opt. Soc. Am. B* **29**, 2516 (2012).
- [50] V. F. Gili, L. Carletti, A. Locatelli, D. Rocco, M. Finazzi, L. Ghirardini, I. Favero, C. Gomez, A. Lemaître, M. Celebrano, C. De Angelis, and G. Leo, Monolithic AlGaAs second-harmonic nanoantennas, *Opt. Express* **24**, 15965 (2016).
- [51] L. Carletti, A. Locatelli, O. Stepanenko, G. Leo, and C. De Angelis, Enhanced second-harmonic generation from magnetic resonance in AlGaAs nanoantennas, *Opt. Express* **23**, 26544 (2015).